ACS OMEGA

Open Access

http://pubs.acs.org/journal/acsodf

Article

Phase Behavior of the Mixtures of 2- and 3-Components for Poly(styrene-*co*-octafluoropentyl methacrylate) by Dispersion Polymerization under CO_2

Uma Sankar Behera, Divya Baskaran, and Hun-Soo Byun*

Cite This: *ACS Omega* 2024, 9, 11910−11924

Read Online

ACCESS | Metrics & More | Article Recommendations

ABSTRACT: The dispersed-phase polymerization of poly(styrene-*co*-2,2,3,4,4,4-octafluoropentyl methacrylate), also known as p(styrene-*co*-OFPMA), took place in supercritical carbon dioxide (sc-CO_2). The chemical and physical properties of p(styrene-*co*-OFPMA) were studied by varying the styrene-to-OFPMA ratios (40:1, 30:1, and 20:1) and 2,2′-azobis(isobutyronitrile) (AIBN) initiator amounts (wt %: 1.0, 2.0, 3.0). The cloud-point data were obtained for various systems, including the binary mixtures of p(styrene-*co*-OFPMA) (30:1 ratio, AIBN wt %: 1.0, 2.0, 3.0) with supercritical solvents such as sc-CO_2, sc-CH_3OCH_3, sc-C_3H_6, sc-C_4H_8, and sc-$CHClF_2$. Phase behavior (i.e., mixtures) was studied at temperatures of 324−455 K and pressure below 201 MPa. In the binary system of p(styrene-*co*-OFPMA) + sc-CH_3OCH_3, a lower critical solution temperature (LCST)-type curve was observed, characterized by a positive slope. Conversely, the binary systems of p(styrene-*co*-OFPMA) + (sc-C3H$_6$, sc-C_4H_8, sc-$CHClF_2$) exhibited an upper critical solution temperature (UCST) behavior with a decreasing slope. The phase equilibrium curves were obtained for p(styrene-*co*-OFPMA) [30:1; 1.0% (M_w = 42,400), 2.0% (M_w = 33,800), and 4.0% (M_w = 24,100); AIBN: 1.0 wt %] + sc-C_3H_6, sc-C_4H_8, and sc-$CHClF_2$ mixtures. These curves exhibited an increasing slope for p(styrene-*co*-OFPMA) + sc-CH_3OCH_3 and a negative slope for p(styrene-*co*-OFPMA) + (sc-C_3H_6, sc-C_4H_8, sc-$CHClF_2$) systems, indicating distinct phase behavior. Tetramethyl orthosilicate (TMOS) addition (0.0−68.9 wt %) to P(styrene-*co*-OFPMA) (30:1; AIBN wt %: 1.0) + solvents altered the phase equilibrium, switching from UCST to LCST, as evidenced by changes in the pressure−temperature slope.

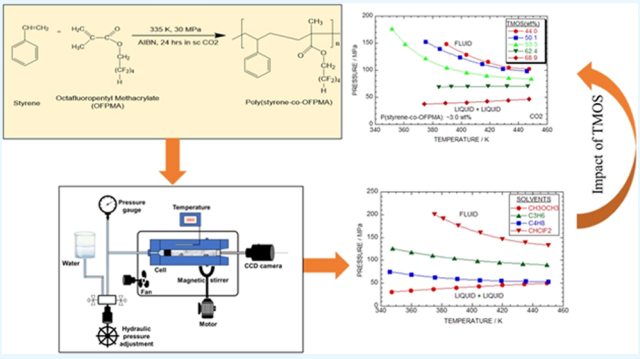

1. INTRODUCTION

The phase transition behavior of mixtures utilizing carbon dioxide (CO_2) as the solvent is of great significance in the development and optimization of supercritical processes. Understanding the phase equilibrium of CO_2-based systems is vital for assessing the feasibility and evaluating the optimal conditions for various processes. By studying the phase equilibrium, including phase transitions, solubility, and critical points, valuable insights can be gained into the system's thermodynamic properties and its potential applications. Polymer blends manifest diverse coexistence phenomena, encompassing upper critical solution temperatures (UCSTs), lower critical solution temperatures (LCSTs), and a hybrid of both. The terminology designates the critical temperature as the UCST when phase separation ensues at temperatures beneath this threshold. Conversely, it is termed the LCST when phase separation unfolds at temperatures surpassing the critical point. This classification delineates the intricate temperature-dependent phase behaviors inherent in polymer mixtures, elucidating critical temperature distinctions that dictate their solubility characteristics. This knowledge enables researchers and engineers to design and optimize supercritical processes more effectively, considering factors such as temperature (T), pressure (p), and composition, thereby advancing the field of supercritical technology. Extensive research has been dedicated to investigating the phase transition behavior of CO_2^+ solute systems at high T and p, as comprehensively reviewed by many researchers.[1−3] These studies have focused on characterizing the phase transitions, solubility, and critical phenomena associated with CO_2-based solvent systems. The findings from these works provide valuable insights and serve as a foundation for understanding the behavior of CO_2^+ solute mixtures, thereby facilitating the

Received: December 4, 2023
Revised: February 6, 2024
Accepted: February 9, 2024
Published: February 26, 2024

Table 1. Specifications of the Chemicals Used

chemical name	mass fraction purity	source	CAS registry number
CO_2	>0.999	Deokyang Gas Co.	124−38−9
styrene	>0.985	Sigma-Aldrich Co.	80−62−6
3,3,4,4,5,5,6,6,7,7,8,8,9,9,10,10,10-heptadecafluorodecyl methacrylate	>0.970	Sigma-Aldrich Co.	1996−88−9
octafluoropentyl methacrylate	>0.980	Sigma-Aldrich Co.	36405−47−7
2,2′-azobisisobutyronitrile	>0.980	Junsei Chemical Co.	78−67−1
1-butene	>0.999	Daehan Gas Co.	106−98−9
propylene	>0.999	Daehan Gas Co.	115−07−1
dimethyl ether	>0.999	Daehan Gas Co.	115−10−6
chlorodifluoromethane	>0.999	Daehan Gas Co.	75−45−6
tetramethyl orthosilicate	>0.980	Sigma-Aldrich Co.	681−84−5
tetraethyl orthosilicate	>0.990	Sigma-Aldrich Co.	78−10−4

design and optimization of various processes involving supercritical carbon dioxide (sc-CO_2).

In recent years, research efforts have shown the promise of utilizing sc-CO_2 as a replacement for traditional hydrocarbon solvents in polymer synthesis and copolymerization processes. This is due to its environmentally friendly nature, cost-effectiveness, and nonflammable properties.[2−4] Polymer synthesis using sc-CO_2 as a pressurizing medium has emerged as a viable approach for obtaining copolymers and polymer products. This process enables the production of polymers and copolymers with desirable properties. The phase behavior exhibited by diverse organic materials and the observed cloud-point phenomenon in certain polymers upon exposure to sc-CO_2 have driven extensive research in the field of radical polymerizations, with particular emphasis on dispersed-phase polymerizations. Dispersed-phase polymerization is a process wherein the initiator and monomer exhibit solubility in the reaction solvent, while the resulting polymer demonstrates insolubility. In the case of dispersion polymerization conducted under sc-CO_2 conditions, specialized stabilizers must be employed to facilitate the process.[5,6] These stabilizers are carefully designed to ensure efficient dispersion of the monomer and initiator within the sc-CO_2 medium, allowing for effective polymerization while preventing agglomeration or coalescence of the expanding polymer units.[7,8] The presence of these tailored stabilizers helps maintain the dispersed state of the polymer units throughout the reaction, enabling the production of well-defined polymer nanoparticles or microspheres with controlled size and morphology. This tailored approach is crucial for achieving desired product properties and optimizing the efficiency of dispersed-phase polymerization in the presence of sc-CO_2. DeSimone reported that 1,1-dihydroperfluorooctyl acrylate, a highly CO_2 soluble stabilizer, was used to disperse-polymerize methyl methacrylate in sc-CO_2.[9] Yuvaraj et al.[10] demonstrated that copolymers containing fluorinated octafluoropentyl methacrylate (OFPMA) and dimethylaminoethyl methacrylate (DMAEMA), known as P(OFPMA-*co*-DMAEMA), exhibited exceptional stabilization effects in the dispersed-phase polymerization in CO_2 of methyl methacrylate (MMA), leading to the formation of abnormally large poly(methyl methacrylate) (PMMA) elements.

Some of the researchers[11−13] have reported the phase equilibrium of various copolymers in sc-solvents. Research on the phase transition data for the ethylene + poly(butyl acrylate-*co*-ethylene) system, covering a "*T*" range of up to ∼523 K and "*p*" up to ∼180 MPa, has been reported.[11] The cloud-point behavior was studied with respect to butyl acrylate containing 5.2−100 mol %. Hasch et al.[12] presented phase transition data for ethylene + poly(methyl acrylate-*co*-ethylene) mixtures, focusing on "*T*" up to ∼513 K and "*p*" up to ∼260 MPa. The cloud-point behavior was examined with respect to methyl acrylate containing 10−100 mol %. Similarly, another study[13] on phase transition for the copolymer made by polymerization of tetrafluoroethylene (TFE) and hexafluoropropylene (HFP) containing 19.3 mol % HFP units in CF_4, C_3F_8, C_2F_6, $CClF_3$, SF_6, C_3F_6, and CO_2 had been reported at elevated (p, *T*) conditions. The observations were made at p_{max} = 270 MPa and *T* (391, 523) K. This copolymer exhibits a combination of properties from both TFE and HFP, making it useful in various applications due to its unique characteristics, such as high chemical resistance and thermal stability.

In the current studies, multiple fluorinated copolymers were created from styrene and OFPMA using sc-CO_2 with 15 wt % P(HDFDMA), i.e., heptadecafluorodecyl methacrylate, as the surfactant and (1.0−4.0) wt % AIBN, i.e., 2,2-azobis-(isobutyronitrile), as the initiator. The role of the surfactant P(HDFDMA) in this context is to aid in the dispersion of the monomers (styrene and OFPMA) in sc-CO_2. By reducing the IFT (i.e., interfacial tension) between the monomers and sc-CO_2, the surfactant promotes their uniform distribution and increases the efficacy of the polymerization method. Additionally, the surfactant can also influence the properties and morphology of the resulting copolymers.

The p(styrene-*co*-OFPMA) polymer offers a wide range of applications in the biomedical field thanks to its biocompatibility and customizable properties.[14] It is highly suitable for biomedical uses due to its ability to be tailored to specific requirements. Additionally, the polymer's hydrophobic and oleophobic properties make it an excellent choice for textile finishes, enhancing the durability and maintenance of textiles. Overall, p(styrene-*co*-OFPMA) presents versatile solutions for various biomedical and textile applications.[14]

This study mainly focuses on the phase transition behavior of a two-component system containing the copolymer p(styrene-*co*-OFPMA) in supercritical fluorinated solvents with nine different copolymers. The phase transition curves of three-component systems involving p(styrene-*co*-OFPMA) + (propylene, 1-butene, CH_3OCH_3, $CHClF_2$) mixtures, in combination with tetramethyl orthosilicate (TMOS)/tetraethyl orthosilicate (TEOS), were investigated across a wide "*T*" range of 324−455 K and "*p*" ranging from 0.52 to 200.86 MPa. These studies provide valuable insights into the behavior of the polymer, enabling its potential application in diverse fields such as packaging materials, membrane preparation for water treatment, and many others. By understanding the phase

https://doi.org/10.1021/acsomega.3c09665
ACS Omega 2024, 9, 11910−11924

Table 2. Physical Properties of Solvents Used in this Study[a]

solvents	chemical formula	M_w (g/mol)	T_c (K)	P_c (MPa)	ω	α (Å^3)	μ (debye)
carbon dioxide	CO_2	44.01					
1-butene	C_4H_8	56.11	419.6	4.02	0.194	8.24	0.3
propylene	C_3H_6	42.08	364.9	4.60	0.140	6.26	0.4
dimethyl ether	CH_3OCH_3	46.07	400.1	5.40	0.200	5.22	1.3
chlorodifluoromethane	$CHClF_2$	86.47	369.2	4.98	0.221	4.44	1.4
tetramethyl orthosilicate[b,c]	$Si(OCH_3)_4$	152.22	544.7	2.61	0.590		
tetraethyl orthosilicate[b,c]	$Si(OC_2H_5)_4$	208.33	574.8	1.98	0.792		

[a]M_w: molecular weight; T_c: critical temperature; P_c: critical pressure; ω: acentric factor; α: polarizability; μ: dipole moment. [b]The properties of gases and liquids. [c]Sigma-Aldrich Co.

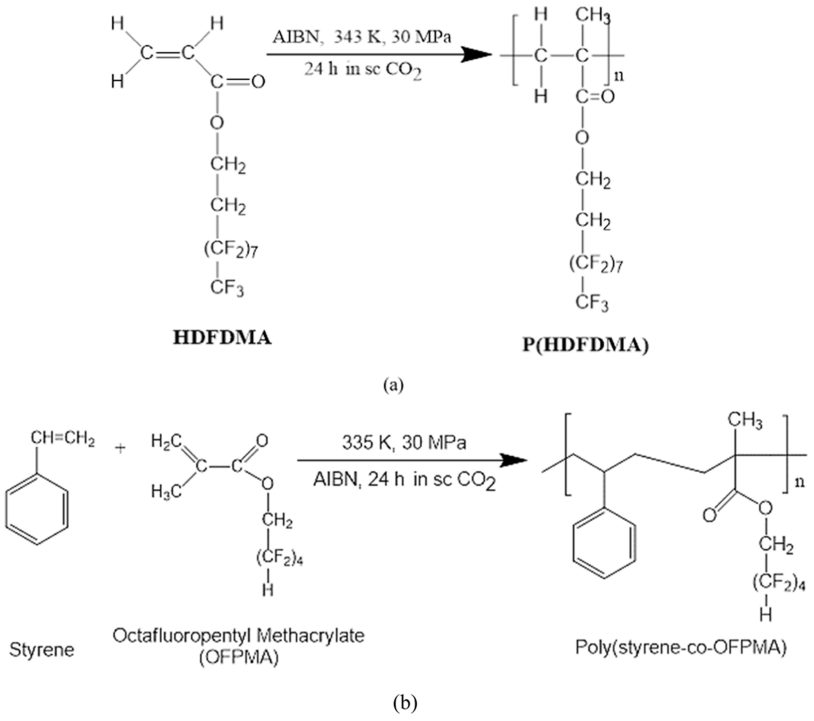

Figure 1. Schematic diagram of the chemical structure of (a) dispersing agent by polymerization for (heptadecafluorodecyl methacrylate) (HDFDMA) and (b) copolymerization for styrene and octafluoropentyl methacrylate (OFPMA).

behavior and characteristics of these ternary systems, we can unlock new possibilities for utilizing p(styrene-*co*-OFPMA) in various industrial and technical implementations.

2. EXPERIMENTAL METHODOLOGY

2.1. Materials. This study includes high-purity materials such as 3,3,4,4,5,5,6,6,7,7,8,8,9,9,10,10,10-heptadecafluorodecyl methacrylate (HDFDMA, >97.0% purity by mass), styrene (>98.5 purity by mass), and 2,2,3,3,4,4,5,5-octafluoropentyl methacrylate (OFPMA, >98.0% purity by mass), which were obtained from Sigma-Aldrich, Ltd. Prior to use, styrene, OFPMA, and HDFDMA were subjected to a pretreatment process involving an alumina column for purification to separate inhibitors and dissolved oxygen if any was eliminated by purging nitrogen gas. The initiator AIBN (98.0% purity by mass) was recrystallized with the help of methanol, purchased from Junsei Chemical.

Propylene (C_3H_6, >99.9% purity by mass), 1-butene (C_4H_8, >99.9% purity by mass), dimethyl ether (DME), and chlorodifluoromethane ($CHClF_2$, >99.9% purity by mass) were acquired from Daehan Gas Ltd., CO_2 (>99.99% purity by mass) was sourced from Deokyang Co. and used as obtained. Table 1 provides a summary of the specifications for all of the chemicals used in the present study. Table 2 presents the properties of the cosolvents and solvents utilized in the present study, as documented by ref 15.

Figure 1 illustrates the diagrammatic representation of the polymerization reaction employed in the present study. In Figure 1(a), the dispersion agent in [P(HDFDMA)] was formulated through uniform solution polymerization. This process involved the polymerization of HDFDMA in sc-CO_2 employing polymerization equipment under controlled conditions (p: 30 MPa with precision 0.3 MPa; T: 338.2 K with precision 0.2 K; AIBN wt %: 1.0). Figure 1(b) shows the synthesis reaction of the p(styrene-*co*-OFPMA) copolymer through dispersion polymerization. The copolymerization process involved varying the ratio of styrene and OFPMA under sc-CO_2 conditions. The polymerization was conducted using a polymerization apparatus with controlled parameters (p: 30 MPa with precision 0.3 MPa; T: 343.2 ± 0.2 K; AIBN wt %: 1.0, 2.0, 4.0).

2.2. Apparatus and Procedure. *2.2.1. Dispersed-Phase Polymerization of Copolymer in sc-CO_2.* The dispersed-phase polymerization of the copolymer in sc-CO_2 was conducted

https://doi.org/10.1021/acsomega.3c09665
ACS Omega 2024, 9, 11910−11924

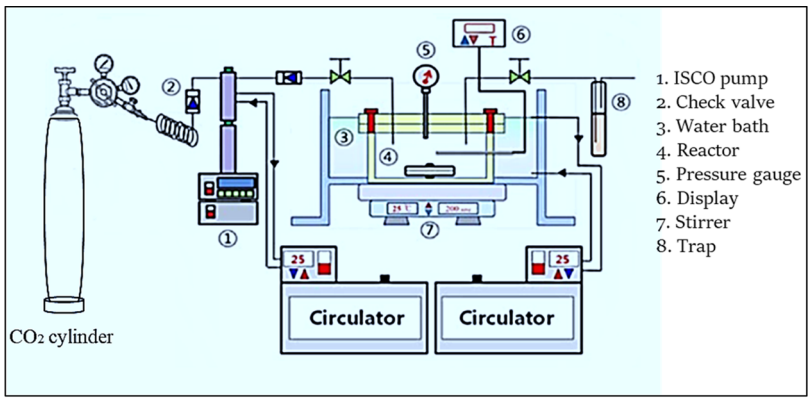

(a)

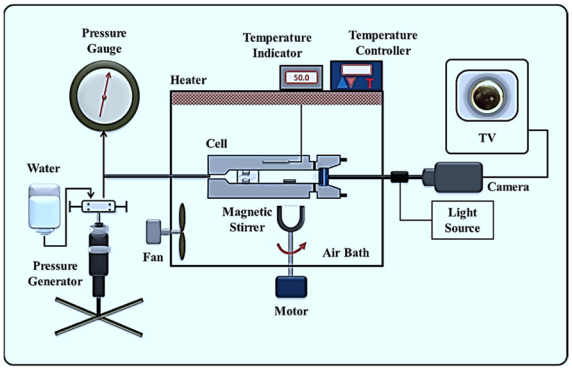

(b)

Figure 2. Schematic diagram of the experimental setup: (a) high-pressure polymerization and (b) high-pressure phase behavior measurement.

Table 3. Copolymers Precipitated According to Mole Ratio of Styrene and OFPMA by Dispersion Polymerization under sc-CO_2

entry	p(styrene-*co*-OFPMA) (wt %)	dispersion agent (wt %)	AIBN (wt %)	[a]M_w (g/mol)	[b]PDI	morphology
40:1	~3.0	15.0	1.0	64,700	2.07	powder
30:1				42,400	1.94	powder
20:1				35,400	2.20	powder
40:1	~3.0	15.0	2.0	49,500	2.90	powder
30:1				33,800	2.25	powder
20:1				26,800	2.94	powder
40:1	~3.0	15.0	4.0	30,080	3.07	powder
30:1				24,100	2.07	powder
20:1				15,500	2.88	powder

[a]M_w is the average molecular weight. [b]PDI is the polydispersity index.

using a high-pressure cylindrical reactor of 30 mL (SUS 316), as depicted in Figure 2(a), and the phase behavior study experimental setup is shown in Figure 2(b). A Bourdon tube "*p*" gauge (model MGS44 DN100, NUOVA FIMA) was arranged to read the "*p*" inside the reactor with a correctness of 1.6 of FSV (full-scale value). An indicator and K-type thermocouple (model NX3, Hanyoung Electronics Inc.) with an accuracy of ±0.5% was used to measure "*T*". To ensure proper mixing, a magnetic stirring bar with polytetrafluoroethylene (PTFE) coated was employed. In the designated reactor, OFPMA and styrene were allowed to react in different mole ratios of 40:1, 30:1, and 20:1 (refer to Table 3 for details) to execute the experiment.

To control the particle sizes, different amounts of 2,2′-azobis(isobutyronitrile) (AIBN; wt %: 1.0, 2.0, 4.0) were added to the p(styrene-*co*-OFPMA) copolymer, as outlined in Tables 4, 5, and 6. P(HDFDMA) was included as the dispersion agent at a concentration of 15 wt %. P(HDFDMA) was developed through uniform radical solution polymerization by subjecting HDFDMA to dispersed-phase polymerization in sc-CO_2 under controlled conditions (*p*: 30 MPa with a precision of 0.3 MPa; *T*: 335.2 K with a precision of 0.2 K; AIBN wt %: 1.0). The reactor was filled with a Teflon-coated stir bar and fully purged with nitrogen and CO_2 to eliminate any air and biological contaminants. The reactor (i.e., high-pressure cell) was pressurized with sc-CO_2 to 7 MPa using an ISCO syringe pump (model 100DX) and after that raised to 323 K. Additional CO_2 was added as the reactor warmed up gradually until the favorable "*p*" and "*T*" conditions of 30 MPa with a precision of 0.3 MPa and 343.2 K with a precision of 0.2 K were reached, respectively. For 24 h, the polymerization process took place with stirring in a sealed reactor. After

https://doi.org/10.1021/acsomega.3c09665
ACS Omega 2024, 9, 11910−11924

Table 4. Experimental Data of Phase Behavior for the p(Styrene-*co*-OFPMA) [30:1, AIBN: (1.0, 2.0 and 4.0) wt %, DA: 15 wt %] + Propylene System

T^a (K)	p^a (MPa)	transition[b]
2.7 wt % p(Styrene-*co*-OFPMA) (AIBN: 1.0 wt %) + 97.3 wt % Propylene		
449.2	89.83	CP
433.4	92.59	CP
418.1	95.69	CP
403.5	98.79	CP
388.3	104.31	CP
373.9	110.52	CP
360.0	118.10	CP
347.6	126.38	CP
3.0 wt % p(Styrene-*co*-OFPMA) (AIBN: 2.0 wt %) + 97.0 wt % Propylene		
448.8	81.55	CP
435.5	82.59	CP
421.7	85.00	CP
406.5	88.10	CP
392.1	92.24	CP
379.2	96.72	CP
365.8	102.59	CP
349.9	110.52	CP
3.4 wt % p(Styrene-*co*-OFPMA) (AIBN: 4.0 wt %) + 96.6 wt % Propylene		
445.4	73.62	CP
428.2	75.17	CP
414.2	76.38	CP
397.0	78.97	CP
384.3	81.03	CP
368.5	85.57	CP
354.7	91.55	CP
343.1	99.14	CP

[a]Standard uncertainties are $u(T)$ = 0.20 K and $u(p)$ = 0.40 MPa. [b]CP: cloud-point; DA: dispersion agent.

Table 5. Experimental Data of Phase Behavior for the p(Styrene-*co*-OFPMA) [30:1, AIBN: 1.0 wt %, DA: 15 wt %] + Propylene + Tetramethyl Orthosilicate System

T^a (K)	p^a (MPa)	transition[b]
2.8 wt % p(Styrene-*co*-OFPMA) (AIBN: 1.0 wt %) + 28.0 wt % TMOS		
449.6	68.45	CP
434.6	68.79	CP
419.1	69.48	CP
405.0	69.83	CP
390.3	70.52	CP
3.1 wt % p(Styrene-*co*-OFPMA) (AIBN: 1.0 wt %) + 29.9 wt % TMOS		
447.2	62.24	CP
432.1	61.90	CP
418.2	61.55	CP
402.6	62.24	CP
388.4	62.93	CP
374.0	63.97	CP
359.3	65.69	CP
345.3	67.76	CP

[a]Standard uncertainties are $u(T)$ = 0.20 K and $u(p)$ = 0.40 MPa. [b]CP: cloud-point; DA: dispersion agent.

completion of the process, the pressure cell "*T*" was reduced to below 288 K, resulting in a solid/gas phase division. CO_2 was gradually liberated from the gaseous state using a glass trap, while the resultant copolymer obtained through dispersed-phase polymerization was gathered and measured in terms of

Table 6. Experimental Data of Phase Behavior for the p(Styrene-*co*-OFPMA) [Mole Ratio: 30:1, AIBN: 1.0 wt %, DA: 15 wt %] + Propylene + ∼30 wt % Tetraethyl Orthosilicate (TEOS) System

T^a (K)	p^a (MPa)	transition[b]
2.6 wt % p(Styrene-*co*-OFPMA) + ∼30 wt % TEOS		
346.5	100.17	CP
360.1	90.52	CP
373.6	84.66	CP
387.9	81.90	CP
402.8	78.79	CP
418.6	76.38	CP
434.6	73.28	CP
451.0	72.24	CP

[a]Standard uncertainties are $u(T)$ = 0.20 K and $u(p)$ = 0.40 MPa. [b]CP: cloud-point; DA: Dispersion agent.

weight. The obtained p(styrene-*co*-OFPMA) copolymer is illustrated in Figure 1(b). The mean molecular weight (M_w) of formulated p(styrene-*co*-OFPMA) was determined using a GPC device, i.e., gel permeation chromatography with a 515 HPLC (water pump) and an ultraviolet (UV) detector (differential refractometer Water 410). It was carried out in a high-resolution column (i.e., Styragel HR4, 300 × 7.8 mm^2, THF). Standards made of polystyrene were used to calibrate M_w values.

2.2.2. Phase Transition Behavior. The experimental setup to analyze the phase transition of the combination of two components and three components of p(styrene-*co*-OFPMA) in sc-CO_2 is shown schematically in Figure 2(b), which is a high-pressure cell. Detailed descriptions of the setup can be found elsewhere.[16−19] A variable-volume view cell that can function at "*p*" up to 300.0 MPa was utilized to measure phase behavior. Supercritical chemical solvents were carefully injected into the vessel with a precision of 0.002 g utilizing an elevated pressure bomb to achieve precise measurements. The empty cell underwent numerous purging cycles with supercritical chemical solvents and nonreactive nitrogen before the measurements to get rid of any lingering traces of air and organic contaminants. The cosolvent monomer was then precisely 0.0008 g added to the reactor using a syringe. A high-pressure system (model 37−5.75−60, HIP) generated pressurized water to displace the piston inside the cell (2.54 cm in length). A Heise gauge (model CM-108952, Dresser Industries) with an accuracy of 0.35 MPa was engaged to read the "*p*" of the mixture. An accurate digital multimeter (Yokogawa, model 7563) and a platinum-resistance thermometer (Class A, Thermometrics Corporation) were engaged to read the cell's "*T*", which is usually kept within the "*T*" limit of 0.2 K. For visualization of the chemical components inside the cell, a camera (borescope, model F100−038−000−50, Olympus Corporation) was positioned against the exterior of the sapphire glass window. This setup facilitated direct observation of the mixture and enabled real-time monitoring of the process on a video monitor. The chemical inside the reactor was subjected to compression until a single phase was achieved while maintaining a constant "*T*". For a permissible time of at least 30−40 min, the equilibrium phase was retained to ensure thermal stability within the target "*T*" range. After that, the "*p*" was slowly reduced until the chemical mixture exhibited cloudiness. The phase transition "*p*" was determined at which the mixture components became sufficiently opaque

https://doi.org/10.1021/acsomega.3c09665
ACS Omega 2024, 9, 11910−11924

that the stirring bar could no longer be seen. Phase transition data were generated at a fixed volume of the copolymer in the homogeneous mixture. The phase transition measurements were performed three times at each "T" condition, with reproducibility typically ±0.28 MPa for "p" and ±0.2 K for "T", and the average value was produced. For a certain cell loading, the predicted combined standard uncertainties for "p" and "T" were 0.40 MPa and 0.20 K, respectively[20,21]

3. RESULTS AND DISCUSSION

3.1. Phase Equilibrium of p(Styrene-*co*-OFPMA) + Solvents Systems. Figure 3 presents the phase equilibrium of

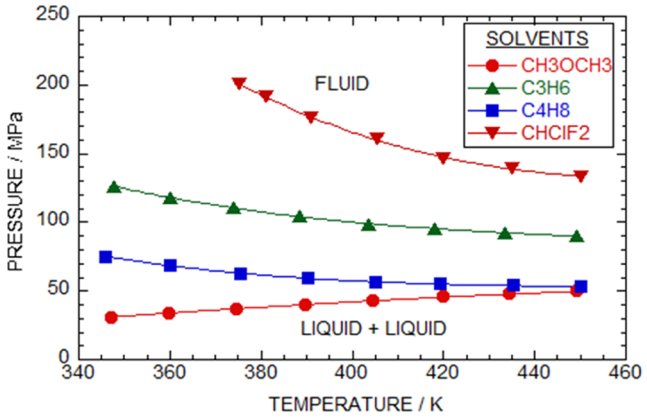

Figure 3. Solvents effects of phase curves for p(styrene-*co*-OFPMA) (mole ratio: 30:1, DA:15 wt %, AIBN: 1.0 wt %) + solvents systems. The concentration of the copolymer is about 3.0 wt % for each solution.

two-component systems consisting of p(styrene-*co*-OFPMA) (30:1; AIBN wt %: 1.0; DA: 15 wt %) mixed in sc-CH_3OCH_3, sc-C_3H_6, sc-C_4H_8, and sc-$CHClF_2$, plotted in the $p-T$ space. The phase equilibrium of the p(styrene-*co*-OFPMA) + $CHClF_2$, C_3H_6, and C_4H_8 systems exhibits an upper critical solution temperature (UCST)-type curve with a declining slope. In contrast, the phase transition behavior of the p(styrene-*co*-OFPMA) + CH_3OCH_3 systems displays lower critical solution temperature (LCST)-type curves with an increasing slope. Figure 3 also demonstrates that the phase transition "p" in CH_3OCH_3 is significantly less compared to the $CHClF_2$ system. The decline in "p" indicates that both density and dispersion interactions play a crucial role in determining phase equilibrium.[21,22] Furthermore, it is noteworthy that despite having similar critical pressure (p_c), the phase transition "p" of the CH_3OCH_3 system is lower compared to the $CHClF_2$ system. This distinction can be attributed to the higher critical temperature and polarizability of CH_3OCH_3, as indicated in Table 2. The data presented in the table are reported in other studies.[22−24]

3.2. Phase Transition Behavior of the p(Styrene-*co*-OFPMA) + C_3H_6 System. Table 4 summarizes the characteristics of the three copolymers (AIBN wt %: 1.0, 2.0, 4.0) formed using a styrene-to-OFPMA ratio of 30:1, while Figure 4 depicts the phase transition behavior for a two-component system of p(styrene-*co*-OFPMA) (30:1) with the sc-solvent.

The two-component system containing p(styrene-*co*-OFPMA) (30:1, AIBN wt %: 1.0; DA wt %: 15; M_w = 42,000) and C_3H_6 exhibits UCST behavior with a declining

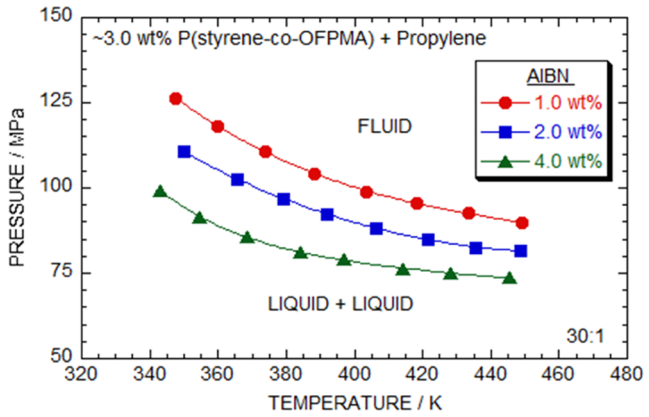

Figure 4. Phase behavior according to AIBN content for the p(styrene-*co*-OFPMA) (mole ratio: 30:1, DA:15%, AIBN: 1.0, 2.0, and 4.0 wt %) + propylene system. The concentration of the copolymer is about 3.0 wt % for each solution.

slope in the "T" range of 347.6− 449.2 K and "p" up to 126.38 MPa.[25]

The phase transition of the p(styrene-*co*-OFPMA) (30:1; AIBN wt %: 2.0; DA wt %: 15, M_w = 33,800) + C_3H_6 mixture displays a negative slope, but only when "p" is below 137.41 MPa and "T" is below 453.5 K. Notably, at "T" above 395 K, the phase transition curve shifts to slightly lower "p", suggesting a decrease in the free volume difference between the solvent and the copolymer.[26,27] At "T" below 395 K, the phase transition behavior exhibits a gradual increase with "p", indicating the prominence of solvent−solvent or copolymer−copolymer polar interactions, leading to phase separation. As a result, the p(styrene-*co*-OFPMA) copolymer tends to precipitate out of the binary system, probably because of the strong copolymer−copolymer interactions. The p(styrene-*co*-OFPMA) (30:1; AIBN wt %: 4.0; M_w = 24100) + C_3H_6 systems exhibit UCST behavior within a "T" limit of 343.1−454.4 K and a "p" maximum of 99.14 MPa.

The phase transition in the (p, T) space of the p(styrene-*co*-OFPMA) (AIBN wt %: 1.0, 2.0, 4.0) + C_3H_6 system, with a cloud-point "p" of 85 ± 4 MPa observed when the "T" reading was 453 K. The phase transition behavior of p(styrene-*co*-OFPMA) (mole ratio = 40:1, 30:1, and 20:1; M_w = 64,7400, 42,400, and 35,400) + C_3H_6 systems exhibits negative slopes at a "T" maximum of 450 K and a "p" maximum of 127 MPa. Notably, below 380 K, the phase transition "p" rises promptly as "T" diminishes, indicating the dominance of solvent−solvent interactions over the interactions between the copolymer and solvent. Due to its dipole moment, C_3H_6 exhibits stronger self-interactions at "T" lower than 363 K (as indicated in Table 2), surpassing the interactions between p(styrene-*co*-OFPMA) and C_3H_6.[22] Moreover, the phase transition behavior of the p(styrene-*co*-OFPMA) + C_3H_6 system exhibit UCST-type behavior within a "p" maximum of 127 MPa and a "T" limit of 343−455 K. Notably, the phase transition "p" of p(styrene-*co*-OFPMA) (AIBN: 4.0 wt %) + C_3H_6 is lower than that of the AIBN wt %: 1.0 and AIBN wt %: 2.0 systems.

Table 5 provides the corresponding experimental data of the p(styrene-*co*-OFPMA) + C_3H_6 + x wt % TMOS system within the "T" limit of 345−450 K and a "p" maximum of 130 MPa, whereas Figure 5 illustrates the phase behavior curve. At a TMOS concentration of 0.0 wt %, the phase transition behavior exhibits a subtle declining slope within the "T" range

https://doi.org/10.1021/acsomega.3c09665
ACS Omega 2024, 9, 11910−11924

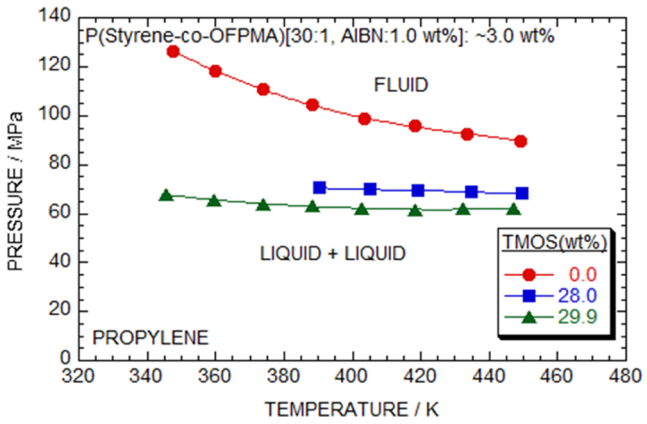

Figure 5. Impact of TMOS concentration for the p(styrene-*co*-OFPMA) (mole ratio: 30:1, DA:15%, AIBN: 1.0 wt %) + propylene + TMOS system. The concentration of the copolymer is about 3.0 wt % for each solution.

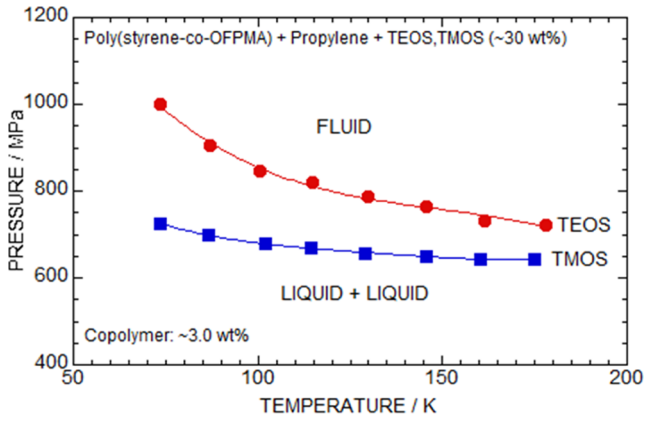

Figure 6. Phase behavior according to TMOS and TEOS (~30 wt %) for the p(styrene-*co*-OFPMA) (mole ratio: 30:1, DA:15%, AIBN: 1.0 wt %) + propylene system. The concentration of the copolymer is about 3.0 wt % for each solution.

of 345−380 K. However, at 390 K, there is an observed decrease in "*p*", which can be attributed to the slower interactions between copolymer segments, surpassing the copolymer−solvent interactions.[28] At a concentration of 28.0 wt %, there is no significant effect observed on the phase transition "*p*". This can be attributed to the low concentration of TMOS, which does not sufficiently enhance the density of the solvent, in this case, C_3H_6, to significantly enhance the quality of the combined solvent. Additionally, the stronger TMOS−TMOS interactions outweigh the slight improvement in favorable dispersion and induced bipolar interactions between propylene and TMOS. Interestingly, with a slight increase in TMOS concentration up to 29.9 wt %, the effective dipole moment of TMOS becomes higher than that of an isolated TMOS molecule. The solvency of the mixed solvent decreases as the amount of TMOS increases due to the solvent's increased polarity. These observations indicate that the concentration of TMOS has a complex influence on the solvent properties and interactions in the system.[29] The addition of TMOS as a cosolvent results in a reduction of the free volume within the solvent, accompanied by an increase in the density of the solvent. As the concentration of TMOS increases, the density of the combined solvent continues to rise. This rise in density facilitates favorable interactions among the copolymer, TMOS cosolvent, and solvent. Consequently, the presence of TMOS leads to a decrease in both "*T*" and "*p*" required for phase separation. The enhanced interactions between the components of the system contribute to the modulation of phase behavior, facilitating the occurrence of phase separation at lower "*T*" and "*p*" conditions.[30−32]

Table 6 represents the investigational data of the three-component system p(styrene-*co*-OFPMA) (30:1, AIBN wt %: 1, DA wt %: 15) + propylene + ~30 wt % tetraethyl orthosilicate (TEOS)/TMOS, and Figure 6 depicts the phase transition curves. The phase transition curve of the ternary system in the presence of TEOS (30 wt %) and TMOS (30 wt %) exhibits UCST-type characteristics with a declining slope. However, the phase transition "*p*" of the ternary mixture p(styrene-*co*-OFPMA) (30:1, AIBN wt %: 1; DA wt %: 15) + propylene + ~30 wt % TEOS is higher than that of p(styrene-*co*-OFPMA) (30:1, AIBN wt %: 1; DA wt %: 15) + propylene + ~30 wt % TMOS, indicating better molecular interactions in the presence of TMOS.[33,34] These results suggest that TMOS has a relatively higher impact on the phase characteristics of the system compared to TEOS.

3.3. Phase Characteristics for the p(Styrene-*co*-OFPMA) + 1-Butene+ TMOS System.

Table 7 and Figure 7 present the phase transition behavior results of the p(styrene-*co*-OFPMA) [DA wt %: 15 + (AIBN wt %: 1.0, 2.0, 4.0), mole ratio: 30:1] mixture dissolved in sc-C_4H_8. As the AIBN concentration is raised from 1 to 4 wt %, the phase behavior of the curve undergoes noticeable changes. However, at all percentages [(1.0−4.0) wt %] of AIBN, the curves exhibit UCST-type behavior with a declining slope with "*p*" between 45 and 78 MPa and a "*T*" range of 333−450 K. At "*T*" above 400 K, there is a moderate shift in the phase transition "*p*" toward approximately 50 MPa. The decrease in the difference in free volume between the copolymer and the solvent is responsible for this shift in the phase transition curve. At "*T*" below 380 K, the phase transition curve shows a gradual increase in "*p*", indicating that phase separation is primarily governed by interactions between copolymer molecules or solvent molecules rather than copolymer−solvent interactions. The strong copolymer−copolymer interactions lead to the precipitation of the p(styrene-*co*-OFPMA) copolymer among the two-component system, resulting in phase separation.[22,35]

Tables 7 and 8 provide the investigational data, and Figure 8 illustrates the phase transition of a two-component system of p(styrene-*co*-OFPMA) with different mole ratios (20:1, 30:1, 40:1) along with a specified AIBN concentration of 2.0 wt % and a DA concentration of 15 wt % in sc-1-butene. The phase transition characteristics of the p(styrene-*co*-OFPMA) [AIBN wt %: 2.0; DA wt %:15; mole ratio: 20:1, 30:1] + 1-butene system overlaps within the "*T*" of 375 to 450 K. All of the curves of different mole ratios are UCST type with declining slopes within "*T*" of 331−455 K and "*p*" less than 75 MPa. The declining slopes suggest that as "*T*" decreases, the phase transition "*p*" increases, indicating an unfavorable state in the dissolvability of the polymer in the solvent.

Table 9 provides experimental data under a "*T*" range of 324−450 K and a "*p*" range of 16−64 MPa, while Figure 9 depicts the phase transition characteristics of the p(styrene-*co*-OFPMA) [AIBN wt %: 1.0, DA wt %: 15, mole ratio: 30:1] + 1-butene + *x* wt % TMOS system. As the TMOS concentration increases to approximately 49.3 wt %, the phase transition curve undergoes a shift from UCST to LCST

https://doi.org/10.1021/acsomega.3c09665
ACS Omega 2024, 9, 11910−11924

Table 7. Experimental Data of Phase Behavior for the p(Styrene-*co*-OFPMA) [Mole Ratio: 30:1, AIBN: (1.0, 2.0 and 4.0) wt %, DA: 15 wt %] + 1-Butene System

T^a (K)	p^a (MPa)	transition[b]
3.0 wt % p(Styrene-*co*-OFPMA) (AIBN: 1.0 wt %) + 97.0 wt % 1-Butene		
450.1	53.28	CP
435.3	53.97	CP
419.4	55.00	CP
405.1	56.72	CP
390.2	59.48	CP
375.5	62.93	CP
360.1	68.45	CP
346.0	75.00	CP
3.0 wt % p(Styrene-*co*-OFPMA) (AIBN: 2.0 wt %) + 97.0 wt % 1-Butene		
454.5	48.45	CP
445.2	48.45	CP
432.9	48.79	CP
424.2	49.14	CP
414.5	49.66	CP
404.9	50.17	CP
392.9	51.38	CP
383.2	53.10	CP
373.6	54.48	CP
360.9	57.24	CP
353.9	60.69	CP
343.2	65.00	CP
334.6	69.31	CP
3.0 wt % p(Styrene-*co*-OFPMA) (AIBN: 4.0 wt %) + 97.0 wt % 1-Butene		
453.8	42.93	CP
438.5	43.28	CP
423.7	43.62	CP
409.4	44.31	CP
394.2	45.00	CP
379.5	46.03	CP
363.6	47.76	CP
348.3	52.59	CP
333.9	59.48	CP

[a]Standard uncertainties are $u(T) = T \pm 0.20$ K and $u(p) = p \pm 0.40$ MPa. [b]CP: cloud-point; DA: dispersion agent.

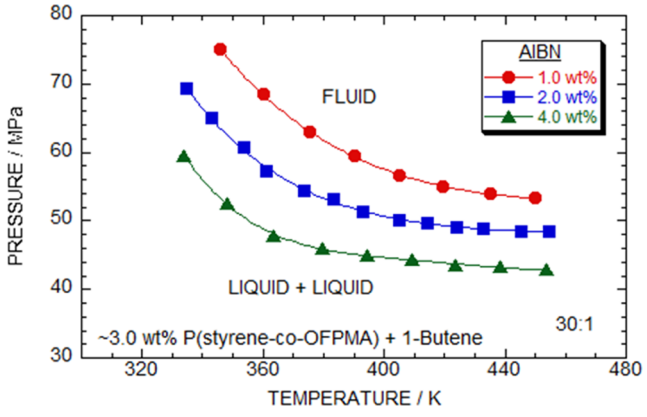

Figure 7. Phase behavior according to AIBN content for the p(styrene-*co*-OFPMA) (mole ratio: 30:1, DA:15%, AIBN: 1.0, 2.0, and 4.0 wt %) + 1-butene system. The concentration of the copolymer is about 3.0 wt % for each solution.

type. Beyond this concentration, the phase transition curve displays a unique U-LCST (upper-lower critical solution temperature) behavior. The distinct U-LCST behavior in the

Table 8. Experimental Data of Phase Behavior for the p(Styrene-*co*-OFPMA) [Mole Ratio: 20:1, 30:1, 40:1, AIBN: 2.0 wt %, DA: 15 wt %] + 1-Butene System

T^a (K)	p^a (MPa)	transition[b]
3.0 wt % p(Styrene-*co*-OFPMA) (20:1) + 97.0 wt % 1-Butene		
331.5	67.41	CP
346.0	62.24	CP
355.3	58.79	CP
365.0	56.38	CP
375.0	54.48	CP
384.4	52.24	CP
394.9	51.55	CP
404.7	50.69	CP
415.4	50.00	CP
423.3	49.66	CP
435.4	49.48	CP
445.2	49.48	CP
452.8	49.14	CP
3.0 wt % p(Styrene-*co*-OFPMA) (40:1) + 97.0 wt % 1-Butene		
334.8	73.45	CP
345.2	66.55	CP
354.2	63.79	CP
361.6	60.69	CP
375.1	57.41	CP
384.0	55.69	CP
394.2	53.79	CP
403.2	53.10	CP
412.2	52.24	CP
426.0	51.38	CP
434.1	51.21	CP
442.4	50.69	CP
455.2	50.17	CP

[a]Standard uncertainties are $u(T) = 0.20$ K and $u(p) = 0.40$ MPa. [b]CP: cloud-point; DA: dispersion agent.

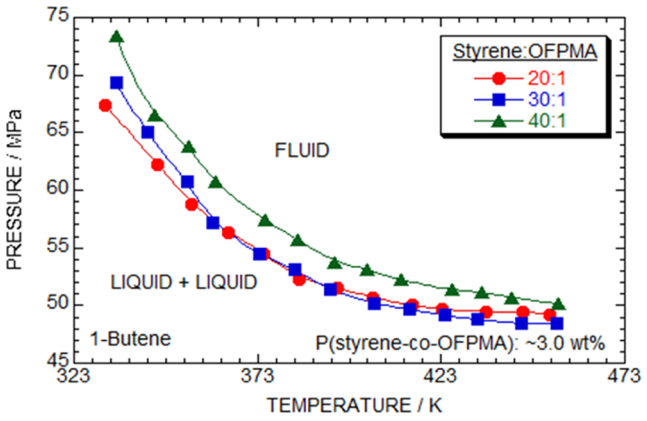

Figure 8. Phase behavior according to the styrene/OFPMA ratio for the p(styrene-*co*-OFPMA) (mole ratio: 40:1, 30:1, 20:1, DA:15%, AIBN: 2.0 wt %) + 1-butene system. The concentration of the copolymer is about 3.0 wt % for each solution.

phase transition curve arises from molecular interactions within the polymer solution. At temperatures below the critical point, the system exhibits UCST, indicating a propensity for phase separation when the temperature drops. This behavior is attributed to the enhanced interactions between the polymer chains or between the polymer and the solvent. Conversely, as the temperature surpasses the critical point, an LCST manifests, signifying a phase transition with increasing

https://doi.org/10.1021/acsomega.3c09665
ACS Omega 2024, 9, 11910−11924

Table 9. Experimental Data of Phase Behavior for the p(Styrene-*co*-OFPMA) [Mole Ratio: 30:1, AIBN: 1.0 wt %, DA: 15 wt %] + 1-Butene + Tetramethyl Orthosilicate (TMOS) System

T^a (K)	p^a (MPa)	transition[b]
2.9 wt % p(Styrene-*co*-OFPMA) (AIBN: 1.0 wt %) + 14.3 wt % TMOS		
446.2	50.17	CP
432.0	50.52	CP
417.7	50.86	CP
402.6	51.55	CP
387.9	53.28	CP
373.9	55.35	CP
358.9	59.14	CP
344.5	63.62	CP
2.9 wt % p(Styrene-*co*-OFPMA) (AIBN: 1.0 wt %) + 29.9 wt % TMOS		
447.4	40.52	CP
431.9	40.17	CP
417.1	39.48	CP
401.3	38.79	CP
386.9	38.45	CP
373.2	39.48	CP
358.9	40.17	CP
344.9	42.24	CP
3.0 wt % p(Styrene-*co*-OFPMA) (AIBN: 1.0 wt %) + 49.5 wt % TMOS		
447.4	28.10	CP
431.2	26.72	CP
416.9	24.66	CP
403.2	22.93	CP
387.9	21.21	CP
373.2	19.48	CP
359.7	18.10	CP
345.1	16.38	CP
2.9 wt % p(Styrene-*co*-OFPMA) (AIBN: 1.0 wt %) + 67.6 wt % TMOS		
448.9	20.17	CP
431.5	17.76	CP
412.5	15.35	CP
397.8	13.28	CP
383.2	10.86	CP
367.5	9.14	CP
355.9	8.45	CP
343.8	8.45	CP
334.5	10.52	CP
324.9	20.17	CP

[a]Standard uncertainties are $u(T)$ = 0.20 K and $u(p)$ = 0.40 MPa. [b]CP: cloud-point; DA: dispersion agent.

temperature. The LCST behavior suggests that at higher temperatures, the intermolecular forces change, leading to decreased solubility and, consequently, phase separation. Furthermore, the phase behavior of the system alters from a temperature-driven phase separation (UCST) to a concentration-driven phase separation (LCST) and then to a combined UCST−LCST type at a TMOS concentration of ∼67.6 wt %. These observations suggest the complex interplay of thermodynamic interactions and molecular structure in the ternary mixture of p(styrene-*co*-OFPMA), 1-butene, and TMOS.[36]

Table 10 and Figure 10 represent the miscibility behavior of the p(styrene-*co*-OFPMA) (DA wt %: 15%, AIBN wt %: 1.0, mole ratio: 30:1) + 1-butene system, covering a "T" range of 372−449 K and a "p" range of 0.52−14 MPa, a wide range of (p, T) conditions. The addition of 74.7 wt % TMOS to the

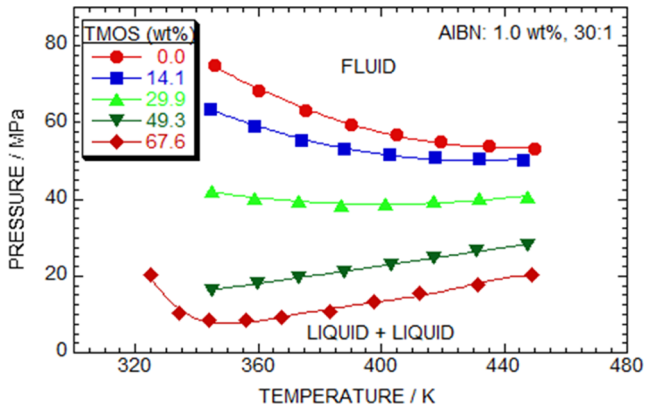

Figure 9. Impact of TMOS concentration for the p(styrene-*co*-OFPMA) (mole ratio: 30:1, DA:15%, AIBN: 1.0 wt %) + 1-butene + TMOS system. The concentration of the copolymer is about 3.0 wt % for each solution.

Table 10. Phase Behavior of CP, BP, and LLV for the p(Styrene-*co*-OFPMA) [Mole Ratio: 30:1, AIBN: 1.0 wt %, DA: 15 wt %] + 1-Butene + Tetramethyl Orthosilicate (TMOS) System

T^a (K)	p^a (MPa)	transition[b]
2.9 wt % p(Styrene-*co*-OFPMA) (AIBN: 1.0 wt %) + 74.7 wt % TMOS		
448.2	13.97	CP
432.8	11.21	CP
418.4	8.45	CP
402.6	6.38	CP
388.3	3.28	CP
372.7	1.06	BP
364.6	0.86	BP
353.7	0.52	BP
390.0	1.59	LLV

[a]Standard uncertainties are $u(T)$ = 0.20 K and $u(p)$ = 0.40 MPa. [b]CP: cloud-point; DA: dispersion agent.

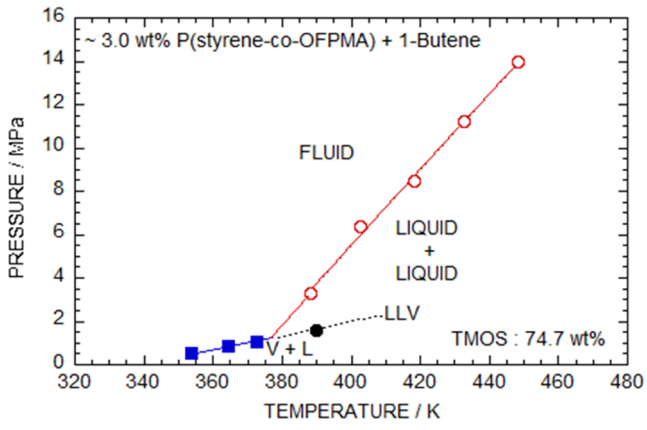

Figure 10. Impact of 74.7 wt % TMOS concentration for the p(styrene-*co*-OFPMA) (mole ratio: 30:1, DA:15%, AIBN: 1.0 wt %) + 1-butene system. The concentration of the copolymer is about 3.0 wt % for each solution.

p(styrene-*co*-OFPMA) (DA wt %: 15%, AIBN wt %: 1.0, mole ratio: 30:1) + 1-butene system resulted in a significant change in phase behavior within the reported "p" and "T" range. Below the curve, a coexistence of liquid and vapor phases was observed. It was anticipated that as the "T" increased from 380

https://doi.org/10.1021/acsomega.3c09665
ACS Omega 2024, 9, 11910−11924

to 420 K, the curve would transition to a liquid + liquid + vapor phase region. However, it was found that a single-phase region could be achieved by operating at higher "T" and lower "p".

3.4. Phase Transition Behavior of the p(Styrene-*co*-OFPMA) + DME System. Table 11 and Figure 11 illustrate the phase transition data and miscibility behavior of the p(styrene-*co*-OFPMA) (AIBN wt %: 1.0, 2.0, 4.0; DA wt %: 15; mole ratio: 30:1) + DME system. The phase transition curves show a distinct change as the AIBN concentration is enhanced from 1.0 to 4.0 wt %. However, across the specified "p" interval of 20−50 MPa and the "T" span of 345−450 K, the curves for all AIBN concentrations are LCST type with an ascending slope. Moreover, by increasing the AIBN concentration in the mixture, the phase transition "p" decreases within a "T" range of 340−450 K. These findings suggest that the presence of AIBN has a significant effect on the phase transition of the p(styrene-*co*-OFPMA) + DME system, enhancing the solubility and promoting better molecular interactions.

Table 11. Experimental Data of Phase Behavior for the p(Styrene-*co*-OFPMA) [Mole Ratio: 30:1, AIBN: (1.0, 2.0 and 4.0) wt %, DA: 15 wt %] + Dimethyl Ether (DME) System

T[a] (K)	p[a] (MPa)	transition[b]
3.0 wt % p(Styrene-*co*-OFPMA) (AIBN: 1.0 wt %) + 97.0 wt % DME		
449.1	49.83	CP
434.5	47.76	CP
419.9	45.69	CP
404.3	42.93	CP
389.6	40.17	CP
374.6	37.09	CP
359.6	33.97	CP
346.9	31.21	CP
3.0 wt % p(Styrene-*co*-OFPMA) (AIBN: 2.0 wt %) + 97.0 wt % DME		
453.4	46.72	CP
437.7	44.31	CP
423.1	41.55	CP
408.1	38.79	CP
394.1	36.03	CP
378.6	33.28	CP
363.5	30.52	CP
348.1	27.41	CP
3.2 wt % p(Styrene-*co*-OFPMA) (AIBN: 4.0 wt %) + 96.8 wt % DME		
444.4	40.52	CP
427.6	37.41	CP
413.1	34.66	CP
397.6	31.90	CP
383.4	29.14	CP
370.2	26.72	CP
356.0	23.28	CP
345.7	20.52	CP

[a]Standard uncertainties are $u(T)$ = 0.20 K and $u(p)$ = 0.40 MPa. [b]CP: cloud-point; DA: dispersion agent.

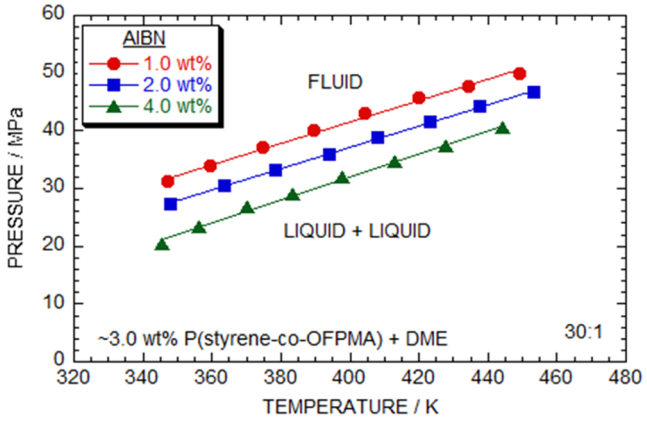

Figure 11. Phase behavior according to AIBN content for the p(styrene-*co*-OFPMA) (mole ratio: 30:1, DA: 15%, AIBN: 1.0, 2.0, and 4.0 wt %) + DME system. The concentration of the copolymer is about 3.0 wt % for each solution.

Table 12 and Figure 12 present the phase equilibrium data (p, T) and the relationship of the p(styrene-*co*-OFPMA) [AIBN wt %: 1.0; DA wt %: 15; mole ratio: 30:1] + TMOS system. The effect of adding TMOS to the p(styrene-*co*-OFPMA) [AIBN wt %: 1.0; DA wt %: 15; mole ratio: 30:1] system while keeping the AIBN concentration fixed at 1.0 wt % was investigated at different TMOS percentages (31.9, 48.8, and 56.9 wt %). The phase equilibrium data demonstrated changes with the addition of TMOS, and the phase behavior of the curve exhibited LCST-type characteristics with increasing slopes. As the concentration of the copolymer in the system increased, the phase transition "p" decreased within the "T" range of 340−450 K. This decrease in phase transition "p" can be attributed to the occupation of the solvent's free volume by the copolymer, leading to enhanced intermolecular interactions.[37,38]

The cloud-point data and phase characteristics of the p(styrene-*co*-OFPMA) (DA wt %: 15, AIBN wt %: 1.0; mole ratio: 30:1) + DME system are presented in Table 13 and Figure 13. The measurements were conducted over a "T" interval of 331−449 K and a "p" span of 0.52−23 MPa. Within these "T" and "p" ranges, a significant change in phase behavior was observed for the p(styrene-*co*-OFPMA) + DME system upon the addition of 60.4 wt % TMOS (mole ratio: 30:1, DA wt %: 15, AIBN wt %: 1.0). Below the curve, the coexistence of the liquid and vapor phases was observed. It was expected that as the "T" increased from 350 to 390 K, the curve would transition to a region of the liquid+liquid+vapor phase. However, further investigation revealed that operating at higher "T" and lower "p" could potentially result in a single-phase region.

3.5. Phase Transition Behavior of the p(Styrene-*co*-OFPMA) + $CHClF_2$ System. The phase characteristics of p(styrene-*co*-OFPMA) (AIBN wt %: 1.0, 2.0, 4.0; DA wt %: 15; mole ratio: 30:1) + $CHClF_2$ systems as discovered in this investigation are given in Table 14 and shown in Figure 14. The phase transition behavior of the p(styrene-*co*-OFPMA) + $CHClF_2$ system exhibits a UCST region in the (p−T) phase diagram (i.e., p−T: pressure−temperature), providing thermodynamic information. At a "T" of 405 K, there is an approximate 26 MPa "p" difference, likely due to differences in M_w, as produced in Table 14. Additionally, the phase transition "p" of p(styrene-*co*-OFPMA) (30:1, AIBN wt %: 1.0, 2.0, 4.0) + $CHClF_2$ mixtures shows an increase in "p" within the p−T space, exhibiting a UCST-type behavior with declining slopes as M_w increases from 352 to 453 K and a maximum "p" of 201 MPa. In Figure 14, the three curves demonstrate the same UCST behavior with increasing M_w and show similar "p" changes as "T" falls inside the p−T region.

https://doi.org/10.1021/acsomega.3c09665
ACS Omega 2024, 9, 11910−11924

Table 12. Experimental Data of Phase Behavior for the p(Styrene-*co*-OFPMA) [Mole Ratio: 30:1, AIBN: 1.0 wt %, DA: 15 wt %] + Dimethyl Ether + Tetramethyl Orthosilicate System

T^a (K)	p^a (MPa)	transition[b]
3.0 wt % p(Styrene-*co*-OFPMA) + 31.9 wt % TMOS		
448.6	36.72	CP
434.4	34.66	CP
418.5	31.90	CP
404.1	29.48	CP
389.1	26.03	CP
374.3	23.28	CP
359.9	20.17	CP
349.1	18.10	CP
2.8 wt % p(Styrene-*co*-OFPMA) + 48.8 wt % TMOS		
447.8	28.79	CP
434.0	26.72	CP
418.6	23.62	CP
403.7	20.52	CP
388.0	17.07	CP
374.5	14.31	CP
360.1	10.86	CP
346.7	7.759	CP
2.7 wt % p(Styrene-*co*-OFPMA) + 56.9 wt % TMOS		
450.1	24.66	CP
434.6	21.90	CP
419.7	19.14	CP
404.0	15.69	CP
387.5	12.59	CP
375.3	9.48	CP
358.6	5.69	CP
339.5	1.21	CP
2.9 wt % p(Styrene-*co*-OFPMA) + 60.4 wt % TMOS		
448.5	22.59	CP
433.5	20.17	CP
418.2	17.76	CP
403.7	14.66	CP
388.6	11.21	CP
373.3	7.76	CP
359.2	3.97	CP
350.2	1.55	CP
340.2	0.86	CP
331.1	0.52	CP

[a]Standard uncertainties are $u(T) = T \pm 0.20$ K and $u(p) = p \pm 0.40$ MPa. [b]CP: cloud-point; DA: dispersion agent.

The finding highlights that the three curves representing different AIBN concentrations show the same UCST behavior, indicating the consistency of the phase behavior with varying copolymer compositions.

The experimental phase transition data for the aforementioned systems are demonstrated in Tables 14 and 15. Figure 15 demonstrates the phase behavior of a binary mixture comprising p(styrene-*co*-OFPMA) (DA wt %:15; AIBN wt %: 2.0; mole ratio: 40:1, 30:1, 20:1) + TMOS dissolved in sc-$CHClF_2$. The observed phase behavior is characterized by a UCST-type curve, indicating phase separation at higher "*T*".[39,40] The "*T*" increase leads to a decrease in miscibility between the components. Moreover, the phase transition "*p*" shows an increasing trend with an increase in the volume ratio. Specifically, the cloud-point "*p*" is highest for the p(styrene-*co*-OFPMA) (AIBN wt %: 2.0, DA wt %: 15, mole ratio: 40:1) +

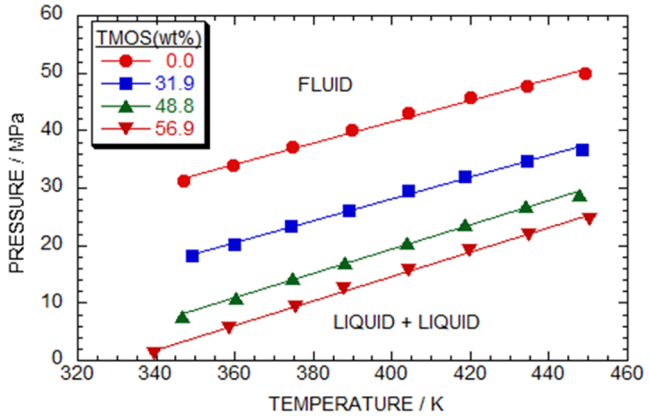

Figure 12. Experimental cloud-point curves for the p(styrene-*co*-OFPMA) [mole ratio: 30:1; AIBN: 1.0 wt %; DA: 15 wt %] + TMOS system dissolved in sc-DME. The concentration of the copolymer is ca. 3.0 for each solution.

Table 13. Experimental Data of Phase Behavior for the p(Styrene-*co*-OFPMA) [Mole Ratio: 30:1, AIBN: 1.0 wt %, DA: 15 wt %] + Dimethyl Ether (DME) + Tetramethyl Orthosilicate (TMOS) System

T^a (K)	p^a (MPa)	transition[b]
2.9 wt % p(Styrene-*co*-OFPMA) + 60.4 wt % TMOS		
448.5	22.59	CP
433.5	20.17	CP
418.2	17.76	CP
403.7	14.66	CP
388.6	11.21	CP
373.3	7.76	CP
359.2	3.97	CP
350.2	1.55	BP
340.2	0.86	BP
331.1	0.52	BP
356.3	1.88	LLV
359.8	2.15	LLV
370.3	2.64	LLV

[a]Standard uncertainties are $u(T) = 0.20$ K and $u(p) = 0.40$ MPa. [b]CP: cloud-point; DA: dispersion agent.

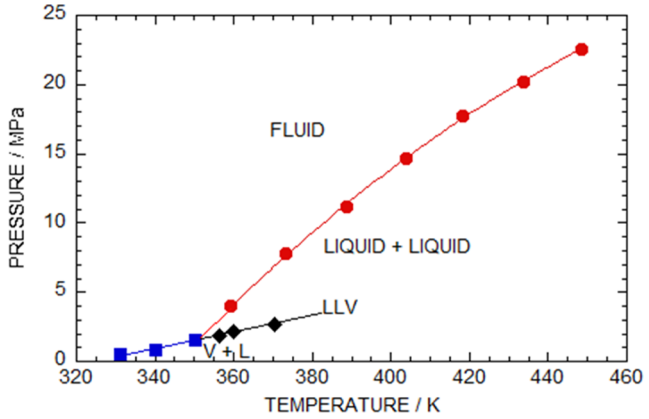

Figure 13. Experimental cloud-point curves for the p(styrene-*co*-OFPMA) [mole ratio: 30:1; AIBN: 1.0 wt %; DA: 15 wt %] + 60.4 wt % TMOS system dissolved in sc-DME. The concentration of the copolymer is about 3.0 wt % of each solution.

https://doi.org/10.1021/acsomega.3c09665
ACS Omega 2024, 9, 11910−11924

Table 14. Experimental Data of Phase Behavior for the p(Styrene-*co*-OFPMA) [Mole Ratio: 30:1, AIBN: (1.0, 2.0 and 4.0) wt %, DA: 15 wt %] + $CHClF_2$ System

T^a (K)	p^a (MPa)	transition[b]
3.0 wt % p(Styrene-*co*-OFPMA) (AIBN: 1.0 wt %) + 97.0 wt % $CHClF_2$		
450.2	133.62	CP
435.0	139.14	CP
419.9	146.72	CP
405.3	160.86	CP
390.9	176.03	CP
381.1	191.21	CP
375.0	200.86	CP
3.1 wt % p(Styrene-*co*-OFPMA) (AIBN: 2.0 wt %) + 96.9 wt % $CHClF_2$		
452.7	116.03	CP
439.3	119.03	CP
432.1	122.24	CP
425.0	124.66	CP
415.7	127.76	CP
404.8	134.83	CP
395.0	141.38	CP
385.0	149.31	CP
374.3	160.52	CP
363.2	176.03	CP
356.6	191.55	CP
2.8 wt % p(Styrene-*co*-OFPMA) (AIBN: 4.0 wt %) + 97.2 wt % $CHClF_2$		
448.2	100.52	CP
432.8	102.59	CP
417.9	105.34	CP
403.9	108.45	CP
389.2	111.90	CP
375.0	118.10	CP
363.0	124.66	CP
352.8	131.21	CP

[a]Standard uncertainties are $u(T) = 0.20$ K and $u(p) = 0.40$ MPa. [b]CP: cloud-point; DA: dispersion agent.

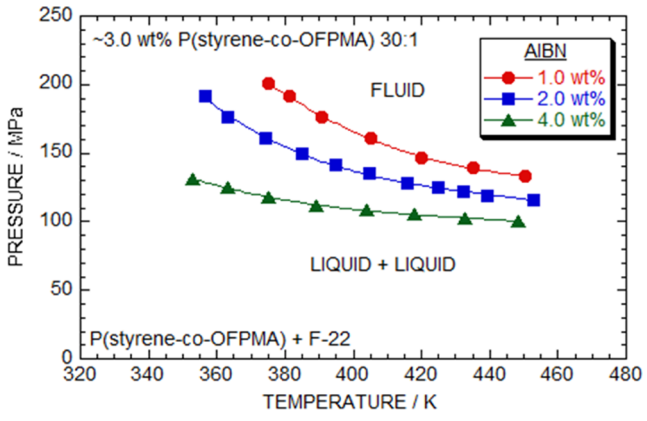

Figure 14. Experimental cloud-point curves for p(styrene-*co*-OFPMA) [mole ratio: 30:1, AIBN: (1.0, 2.0 and 4.0) wt %; DA: 15 wt %] dissolved in sc-$CHClF_2$. The concentration of the copolymer is ca. 3.0 for each solution.

TMOS system, while it is lowest for the p(styrene-*co*-OFPMA) (AIBN wt %: 2.0, DA wt %: 15 mol ratio: 20:1) + TMOS system.

Table 16 and Figure 16 depicts the phase equilibrium curve of the p(styrene-*co*-OFPMA) (mole ratio: 30:1, DA wt %: 15%, AIBN wt %: 1.0) + *x* wt % TMOS system in sc-CO_2 under varying "*p*" (37 to 178 MPa) and "*T*" (350 to 450 K)

Table 15. Experimental Data of Phase Behavior for the p(Styrene-*co*-OFPMA) [Mole Ratio: 20:1, 30:1, 40:1, AIBN: 2.0 wt %, DA: 15 wt %] + $CHClF_2$ System

T^a (K)	p^a (MPa)	transition[b]
2.7 wt % p(Styrene-*co*-OFPMA) (20:1) + 97.3 wt % $CHClF_2$		
345.0	124.65	CP
353.5	123.67	CP
372.6	113.10	CP
384.8	108.10	CP
394.4	105.34	CP
415.8	98.62	CP
425.3	97.07	CP
435.2	96.03	CP
445.2	94.48	CP
454.4	93.62	CP
2.8 wt % p(Styrene-*co*-OFPMA) (40:1) + 97.2 wt % $CHClF_2$		
374.0	197.24	CP
385.5	179.83	CP
393.5	168.16	CP
400.3	159.83	CP
414.0	149.31	CP
423.5	141.90	CP
436.1	135.00	CP
445.8	130.00	CP
452.5	127.41	CP

[a]Standard uncertainties are $u(T) = T \pm 0.20$ K and $u(p) = p \pm 0.40$ MPa. [b]CP: cloud-point; DA: dispersion agent.

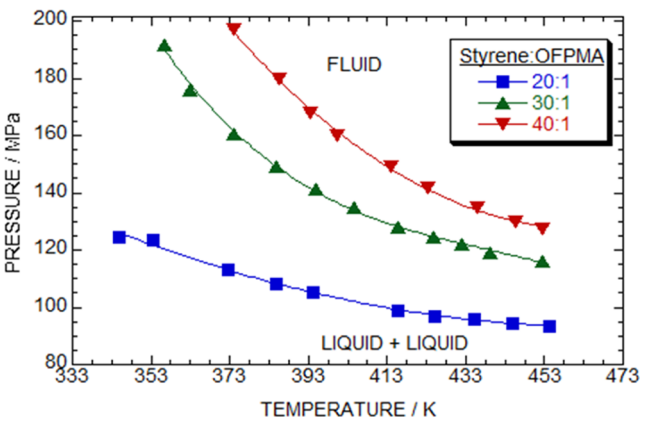

Figure 15. Experimental cloud-point curves for the p(styrene-*co*-OFPMA) [mole ratio: 40:1, 30:1, 20:1, AIBN: 2.0 wt %, DA: 15 wt %] + TMOS system dissolved in sc-$CHClF_2$. The concentration of the copolymer is 3.0 wt % for each solution.

conditions. The characteristics of the phase equilibria curves shift from UCST type with declining slopes to LCST type with increasing slopes as the wt % of TMOS increases (from 44.0 to 68.9). The p(styrene-*co*-OFPMA) (mole ratio: 30:1, DA wt %: 15, AIBN wt %: 1.0) + (44.0, 50.1, 53.3) wt % TMOS systems exhibit UCST behavior with negative slopes, while the p(styrene-*co*-OFPMA) (mole ratio: 30:1, DA wt %: 15, AIBN wt %: 1.0) + (68.9) wt % TMOS system shows LCST-type behavior with positive slopes. However, the p(styrene-*co*-OFPMA) mole ratio: 30:1, DA wt %: 15%, AIBN wt %: 1.0 + 62.4 wt % TMOS system exhibits a neutral behavior within the studied experimental conditions. TMOS diminishes the available space within the solvent and enhances its density due to the significantly higher density of TMOS compared to CO_2. The increase in cosolvent content leads to a

https://doi.org/10.1021/acsomega.3c09665
ACS Omega 2024, 9, 11910−11924

Table 16. Experimental Data of the p(Styrene-*co*-OFPMA) [Mole Ratio: 30:1, AIBN: 2.0 wt %, DA: 15 wt %] + CO_2 + Tetramethyl Orthosilicate (TMOS) System

T^a (K)	p^a (MPa)	transition[b]
2.6 wt % p(Styrene-*co*-OFPMA) + 44.0 wt % TMOS		
447.45	102.93	CP
433.10	105.00	CP
418.65	115.34	CP
403.55	128.45	CP
389.55	148.45	CP
2.9 wt % p(Styrene-*co*-OFPMA) + 50.1 wt % TMOS		
445.95	98.79	CP
429.15	102.93	CP
414.55	111.21	CP
399.15	123.62	CP
384.95	139.48	CP
375.15	152.59	CP
2.8 wt % p(Styrene-*co*-OFPMA) + 53.3 wt % TMOS		
449.00	84.66	CP
433.25	86.38	CP
417.75	90.17	CP
403.95	96.03	CP
389.85	104.66	CP
375.05	121.90	CP
361.10	148.45	CP
351.65	177.41	CP
2.9 wt % p(Styrene-*co*-OFPMA) + 62.4 wt % TMOS		
446.55	70.86	CP
432.05	70.52	CP
418.55	70.17	CP
404.45	69.83	CP
393.15	69.48	CP
384.55	69.14	CP
3.3 wt % p(Styrene-*co*-OFPMA) + 68.9 wt % TMOS		
447.20	46.72	CP
432.90	44.31	CP
417.95	42.93	CP
403.95	40.17	CP
389.20	39.14	CP
374.25	37.76	CP

[a]Standard uncertainties are $u(T)$ = 0.20 K and $u(p)$ = 0.40 MPa. [b]CP: cloud-point; DA: dispersion agent.

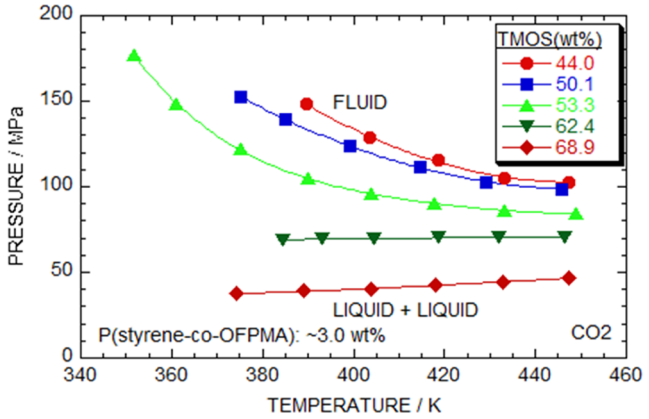

Figure 16. Phase behavior according to the p(styrene-*co*-OFPMA) (mole ratio:30:1, DA:15%, AIBN: 1.0 wt %) + TMOS system under sc-CO_2. The concentration of the copolymer is about 3.0 wt % for each solution.

higher density of the mixed solvent and favorable interactions among the solvent, copolymer, and cosolvent, resulting in lower "*T*" and "*p*" conditions.[41−43]

4. CONCLUSIONS

This study investigated the phase transition of p(styrene-*co*-OFPMA) in two- and three-component systems utilizing supercritical fluids. The p(styrene-*co*-OFPMA) copolymers were synthesized through dispersion polymerization in sc-CO_2. The characterization of p(styrene-*co*-OFPMA) copolymers involved varying the mole ratio of styrene to OFPMA (40:1, 30:1, 20:1) and the AIBN concentration (AIBN wt %: 1.0, 2.0, 4.0).

The phase transition behavior of p(styrene-*co*-OFPMA) was investigated in binary and ternary mixtures with sc-C_3H_6, 1-butene, DME, CO_2, and $CHClF_2$. The results showed that p(styrene-*co*-OFPMA) + C_3H_6, 1-butene, and $CHClF_2$ exhibited UCST-type behavior with a declining slope, indicating phase separation at higher "*T*". On the other hand, p(styrene-*co*-OFPMA) + DME displayed LCST-type behavior with an increasing slope, suggesting phase separation at lower "*T*".

Furthermore, the influence of TMOS on the (*p*, *T*) relationship of p(styrene-*co*-OFPMA) + *x* wt % TMOS under sc-CO_2 (30:1; AIBN wt %: 1.0, 2.0) was investigated. It was observed that as the concentration of TMOS in the mixtures increased, the (*p*, *T*) slope shifted from a UCST-type curve to an LCST-type curve.

To sum up, a solvent with a distinct phase transition offers accurate regulation of separation, precipitation, and particle creation processes. This demarcation between polymer solubility regions enhances efficiency and predictability, which holds significant importance in various industries.

AUTHOR INFORMATION

Corresponding Author

Hun-Soo Byun − *Department of Chemical and Biomolecular Engineering, Chonnam National University, Yeosu, Jeonnam 59626, South Korea;* orcid.org/0000-0003-2356-8515; Phone: +82-61-659-7296; Email: hsbyun@jnu.ac.kr; Fax: +82-61-653-3659

Authors

Uma Sankar Behera − *Department of Chemical and Biomolecular Engineering, Chonnam National University, Yeosu, Jeonnam 59626, South Korea;* orcid.org/0000-0002-1388-0401

Divya Baskaran − *Department of Chemical and Biomolecular Engineering, Chonnam National University, Yeosu, Jeonnam 59626, South Korea*

Complete contact information is available at: https://pubs.acs.org/10.1021/acsomega.3c09665

Notes

The authors declare no competing financial interest.

ACKNOWLEDGMENTS

This work was supported by the National Research Foundation of Korea (NRF) grant funded by the Korean government (MSIT) (No. 2021R1A2C2006888).

https://doi.org/10.1021/acsomega.3c09665
ACS Omega 2024, 9, 11910−11924

REFERENCES

(1) Fornari, R. E.; Alessi, P.; Kikic, I. High pressure fluid phase equilibria: experimental methods and systems investigated (1978−1987). *Fluid Phase Equilib.* **1990**, *57*, 1−33, DOI: 10.1016/0378-3812(90)80010-9.

(2) Dohrn, R.; Brunner, G. High-pressure fluid-phase equilibria: Experimental methods and systems investigated (1988−1993). *Fluid Phase Equilib.* **1995**, *106*, 213−282.

(3) Christov, M.; Dohrn, R. High-pressure fluid phase equilibria: Experimental methods and systems investigated (1994−1999). *Fluid Phase Equilib.* **2002**, *202*, 153−218.

(4) Matsukawa, H.; Fujii, A.; Hoshina, T.; Otake, K. Pressure−Volume−Temperature Relationships of Tetraethyl, Tetrapropyl, and Tetrabutyl Orthosilicates. *J. Chem. Eng. Data* **2022**, *67*, 14−22.

(5) Ding, L.; Olesik, S. V. Dispersion polymerization of MMA in supercritical CO_2 in the presence of copolymers of perfluorooctylethylene methacrylate and poly(propylene glycol) methacrylate. *Macromolecules* **2003**, *36*, 4779−4785.

(6) Hwang, H. S.; Lee, W. K.; Hong, S. S.; Jin, S. H.; Lim, K. T. Dispersion polymerization of MMA in the presence of poly(poly(ethylene glycol) methacrylate-*co*-1H,1H,2H,2H-perfluorooctylmethacrylate). *J. Supercrit. Fluids* **2007**, *39*, 409−415.

(7) Lepilleur, C.; Beckman, E. J. Dispersion polymerization of methyl methacrylate in supercritical CO_2. *Macromolecules* **1997**, *30*, 745−756.

(8) Galia, A.; Pierro, P.; Filardo, G. Dispersion polymerization of methyl methacrylate in supercritical carbon dioxide stabilized with poly(ethylene glycol)-b-perfluoroalkyl compounds. *J. Supercrit. Fluids* **2004**, *32*, 255−263.

(9) Hsiao, Y. L.; Maury, E. E.; DeSimone, J. M.; Mawson, S.; Johnston, K. P. Dispersion polymerization of methyl methacrylate stabilized with poly(1,1-dihydroperfluorooctyl acrylate) in supercritical carbon dioxide. *Macromolecules* **1995**, *28*, 8159−8166.

(10) Yuvaraj, H.; Hwang, H. S.; Woo, M. H.; Park, E. J.; Ganapathy, H. S.; Gal, Y. S.; Lim, K. T. Dispersion polymerization of styrene in supercritical CO_2 stabilized by random copolymers of 1*H*,1*H*-perfluorooctyl methacrylate and 2-dimethylaminoethyl methacrylate. *J. Supercrit. Fluids* **2007**, *42*, 359−365.

(11) Byun, H. S.; Hasch, B. M.; McHugh, M. A.; Mahling, F.-O.; Busch, M.; Buback, M. Poly(ethylene-co-butyl acrylate). Phase behavior in ethylene compared to the poly(ethylene-co-methyl acrylate)-ethylene system and aspects of copolymerization kinetics at high pressures. *Macromolecules* **1996**, *29*, 1625−1632.

(12) Hasch, B. M.; Meilchen, M. A.; Lee, S.-H.; McHugh, M. A. High-Pressure phase behavior of mixtures of poly(ethylene-co-methyl acrylate) with low-molecular weight hydrocarbons. *J. Polym. Sci., Part B: Polym. Phys.* **1992**, *30*, 1365−1373.

(13) Mertdogan, C. A.; Byun, H. S.; McHugh, M. A.; Tuminello, W. H. Solubility of poly(tetrafluoroethylene-co-19 mol% hexafluoropropylene) in supercritical CO_2 and halogenated supercritical solvents. *Macromolecules* **1996**, *29*, 6548−6555.

(14) Pollack, K. A.; Imbesi, P. M.; Raymond, J. E.; Wooley, K. L. Hyperbranched fluoropolymer-polydimethylsiloxane-poly (ethylene glycol) cross-linked terpolymer networks designed for marine and biomedical applications: heterogeneous nontoxic antibiofouling surfaces. *ACS Appl. Mater. Interfaces.* **2014**, *6*, 19265−19274.

(15) DiNoia, T. P. Impact of Solvent Quality and Polymer Architecture on Polymer-Supercritical Fluid Solutions: Phase Behavior and Small-Angle Neutron Scattering Investigations. Ph.D. Dissertation, Johns Hopkins University: Baltimore, MD, 2000.

(16) Yoon, S. D.; Jang, Y. S.; Choi, T. H.; Byun, H. S. High pressure phase behavior for the binary mixture of pentafluoropropyl methacrylate and poly(pentafluoropropyl methacrylate) in supercritical carbon dioxide and dimethyl ether. *Korean J. Chem. Eng.* **2012**, *29*, 413−419.

(17) Kwon, Y. T.; Dhamodharan, D.; Choi, H.; Shim, S. W.; Byun, H. S. Experimental and computational phase behavior analysis of the PGME+ CO2 and PGMEA+ CO2 mixture at high pressures. *Korean J. Chem. Eng.* **2022**, *39*, 2783−2791.

(18) Behera, U. S.; Lee, H. S.; Lee, C. W.; Byun, H. S. Understanding the thermodynamic phase equilibria for the allyl acetate, allyl acrylate and allyl methacrylate under CO2 as supercritical solvent. *J. CO_2 Util.* **2023**, *73*, No. 102519.

(19) Ghoderao, P. N.; Lee, C. W.; Byun, H. S. Phase behavior investigation of the vinyl toluene and poly (vinyl toluene) + co-solvents in supercritical CO_2. *J. Ind. Eng. Chem.* **2023**, *121*, 92−99.

(20) Chirico, R. D.; Frenkel, M.; Diky, V. V.; Marsh, K. N.; Wilhoit, R. C. ThermoML-AnXML-based approach for storage and exchange of experimental and criticallyevaluated thermophysical and thermochemical property data. 2. Uncertainties. *J. Chem. Eng. Data* **2003**, *48*, 1344−1359.

(21) Park, C. W.; Kim, C. H.; Byun, H. S. Measurement and modeling for 3-Methoxy-3-Methyl-1-Butanol and 1-Methoxy-2-Methyl-2-Propanol in super critical carbon dioxide. *Korean J. Chem. Eng.* **2021**, *38*, 610−616.

(22) Kim, C. R.; Byun, H. S. Experimental measurement of solubility curves for poly (methyl methacrylate-co-pentafluorophenyl methacrylate) in supercritical solvents. *J. Chem. Thermodyn.* **2016**, *97*, 26−38.

(23) Jammaer, J. A. G.; Mellaerts, R.; Laenen, S.; Thomassen, L.; Augustijns, P.; Van den Mooter, G.; Elst, K.; Van Ginneken, L.; Martens, J. A. Binary phase diagram of tetraethyl orthosilicate and carbon dioxide. *J. Chem. Eng. Data* **2008**, *53*, 2573−2575.

(24) Poling, B. E.; Prausnitz, J. M.; O'Connell, J. P. *Properties of Gases and Liquids*, 5th Ed., McGraw Hill, New York, 2001.

(25) Kirby, C. F.; McHugh, M. A. Phase behavior of polymers in supercritical fluid solvents. *Chem. Rev.* **1999**, *99*, 565−602.

(26) Wolf, B. A.; Blaum, G. Measured and calculated solubility of polymers in mixed solvents: monotory and cosolvency. *J. Polym. Sci., Part B: Polym. Phys.* **1975**, *13*, 1115−1132.

(27) McHugh, M. A.; Krukonis, V. J. *Supercritical Fluid Extraction: Principles and Practice*, 2nd ed.; Butterworth: MA, 1994.

(28) Rindfleisch, F.; DiNoia, T. P.; McHugh, M. A. Solubility of polymers and copolymers in supercritical CO_2. *J. Phys. Chem.,* **1996**, *100*, 15581−15587.

(29) Patterson, D. Role of free volume in polymer solution thermodynamics. *Pure Appl. Chem.* **1972**, *31*, 133−149.

(30) Whaley, P. D.; Winter, H. H.; Ehrlich, P. Phase equilibria of polypropylene with compressed propane and related systems. 1. Isotactic and atactic polypropylene with propane and propylene. *Macromolecules* **1997**, *30*, 4882−4886.

(31) Patterson, D. Free volume and polymer solubility. A qualitative view. *Macromolecules* **1969**, *2*, 672−677.

(32) Byun, H. S.; Kim, C. R.; Yoon, S. D. Cloud-point measurement of binary and ternary mixtures for the P (MMA-co-PnFPA) in supercritical fluoric solvents. *J. Supercrit. Fluids* **2017**, *120*, 226−239.

(33) Ding, Y.; Zhang, X.; Xu, B.; Li, W. LCST and UCST-type thermoresponsive behavior in dendronized gelatins. *Polym. Chem.* **2022**, *13*, 2813−2821.

(34) Dong, Z.; Mao, J.; Wang, D.; Yang, M.; Wang, W.; Bo, S.; Ji, X. Tunable dual-thermoresponsive phase behavior of zwitterionic polysulfobetaine copolymers containing poly (N, N-dimethylaminoethyl methacrylate)-grafted silica nanoparticles in aqueous solution. *Macromol. Chem. Phys.* **2014**, *215*, 111−120.

(35) Cho, S. H.; Kim, C. R.; Yoon, S. D.; Byun, H. S. Phase behavior and characterization of the poly (methyl methacrylate-co-octafluoropentyl methacrylate) [P (MMA-co-OFPMA)] by supercritical dispersion polymerization. *Fluid Phase Equilib.* **2015**, *396*, 74−87.

(36) Lanza, M.; Ndiaye, P. M.; Tavares, F. W.; Oliveira, D.; Dariva, C.; Oliveira, J. V. Phase behavior of castor oil in compressed propane and n-butane. *J. Supercrit. Fluids* **2005**, *34*, 215−221.

(37) Behera, U. S.; Prasad, S. K.; Byun, H. S. Experimental validation on the phase separation for the 2-(Diisopropylamino) ethyl methacrylate and Poly [2-(diisopropylamino) ethyl methacrylate] in supercritical CO2. *J. Mol. Liq.* **2024**, *393*, No. 123553.

(38) Behera, U. S.; Prasad, S. K.; Baskaran, D.; Byun, H. S. Phase behavior of biodegradable poly (L-lactic acid) in supercritical solvents and cosolvents. *J. CO_2 Util.* **2024**, *79*, No. 102658.

https://doi.org/10.1021/acsomega.3c09665
ACS Omega 2024, 9, 11910−11924

(39) Swier, S.; Van Mele, B. In situ monitoring of reaction-induced phase separation with modulated temperature DSC: comparison between high-Tg and low-Tg modifiers. *Polym. J.* **2003**, *44*, 2689−2699.
(40) Ng, S. C.; Görlich, D. A simple thermodynamic description of phase separation of Nup98 FG domains. *Nat. Commun.* **2022**, *13*, No. 6172.
(41) Rindfleisch, F.; DiNoia, T. P.; McHugh, M. A. Solubility of polymers and copolymers in supercritical CO_2. *J. Phys. Chem. A* **1996**, *100*, 15581−15587.
(42) Prausnitz, J. M.; Lichtenthaler, R. N.; de Azevedo, E. G. *Molecular Thermodynamics of Fluid-Phase Equilibria*, 3rd ed.; Prentice-Hall: Upper Saddle River, NJ, 1999.
(43) Behera, U. S.; Cho, S. H.; Dhamodharan, D.; Byun, H. S. Phase equilibria of binary and ternary mixtures with poly (styrene-co-hexafluorobutyl methacrylate) and solvents at high pressure and temperature. *J. Supercrit. Fluids* **2024**, *205*, No. 106146.

https://doi.org/10.1021/acsomega.3c09665
ACS Omega 2024, 9, 11910−11924